Fuel 304 (2021) 121394

Contents lists available at ScienceDirect

Fuel

journal homepage: www.elsevier.com/locate/fuel

Full Length Article

Effective application of proppants during the hydraulic fracturing of coal seam gas reservoirs: Implications from laboratory testings of propped and unpropped coal fractures

M.A.A. Ahamed [a], M.S.A. Perera [a,*], D. Elsworth [b], P.G. Ranjith [c], S.K.M. Matthai [a], Li Dong-yin [d]

[a] Department of Infrastructure Engineering, Engineering Block B, Grattan Street, Parkville, The University of Melbourne, Victoria 3010, Australia
[b] Energy and Mineral Engineering, G3 Center and EMS Energy Institute, Pennsylvania State University, University Park, PA 16801, USA
[c] Department of Civil Engineering, Monash University, Clayton Campus, Victoria 3800, Australia
[d] School of Energy Science and Engineering, Henan Polytechnic University, Jiaozuo 454000, China

ARTICLE INFO

Keywords:
Coal seam gas
Proppants
Conductivity
Proppant embedment
Surface roughness

ABSTRACT

Commercial production of coal seam gas is a significant proportion of the total Worldwide natural gas supply due to its high gas storage capacity at shallow extraction depths. Coal seam gas recovery may be enhanced by pure fluid-based or proppant based hydraulic fracturing – the decision whether or not to use proppants depends on coal seam characteristics – in particular stress-permeability characteristics. Although proppant application has been common in deep reservoir fracturing, its application on soft rocks such as coal should be carefully investigated. Higher concentrations of proppant are known to minimise proppant damage in deep reservoirs, with stiffness and flow tortuosity also impacting the response. We explored the impact of proppant loading, coal type and fracture roughness on fluid flow characteristics in propped fractures by conducting a series of triaxial permeability experiments combined with micro-CT imaging. The results reveal that proppant application in coal is only effective for deep coal seam gas reservoirs with effective stress greater than 6 to 8 MPa (~700 to ~900 m). Further, proppant application may cause up to 1–2 folds of fracture conductivity improvement in coal seam gas reservoirs located at over 1.2–1.4 km depths (effective stresses > 12 MPa). The impact caused by proppant embedment on fracture conductivity degradation is much significant compared to other proppant damage mechanisms. The effect, however, depends on the stiffness of the coal rock matrix and the proppant type implemented.

1. Introduction

The previous two decades have shown a continuous increase in the consumption of high carbon fossil fuels such as coal and oil, resulting in an increase in energy prices, dwindling energy sources, and increase in the environment pollution. The utilization of natural gas offers some appeal in countering these impacts and is currently the fastest-growing fossil fuel in the World [1–3]. Natural gas is differentiated according to its source: 1) conventional gas - trapped in porous and permeable rocks below a caprock that may be recovered without significant enhancement in reservoir permeability, and 2) unconventional gas - trapped at the point of formation in highly impermeable rocks, such as shales and coals, where permeability enhancement is typically required to enable recovery [4]. Among the unconventional gas resources, coal seam gas is receiving increasing interest due to its lower capital cost, high-density of storage and ready accessibility at relatively shallow depths [5].

While standard techniques such as vertical drilling and conventional dewatering are sufficient to extract conventional gas, these techniques can recover only a fraction of the available gas from unconventional gas reservoirs. Conventional recovery lowers pressure within the reservoir, desorbs the gas from the pore spaces to the cleats, and allows the desorbed gas to flow to the wellbore under the excess pressure [6]. However, coal seam gas is usually trapped in a low permeability matrix, requiring the use of hydraulic fracturing to pre-fracture the reservoir and reduce diffusion lengths from pore to well.

Hydraulic fracturing is typically applied based on threshold initial reservoir permeabilities. Typically, targeted seams have permeabilities between 1 and 20 mD, whereas seams with permeability lower than 0.1

* Corresponding author at: Department of Infrastructure Engineering, Room: B 209, Engineering Block B, Building 175, Grattan Street, Parkville, The University of Melbourne, Victoria 3010, Australia.
E-mail address: samintha.perera@unimelb.edu.au (M.S.A. Perera).

https://doi.org/10.1016/j.fuel.2021.121394
Received 30 March 2021; Received in revised form 4 July 2021; Accepted 5 July 2021

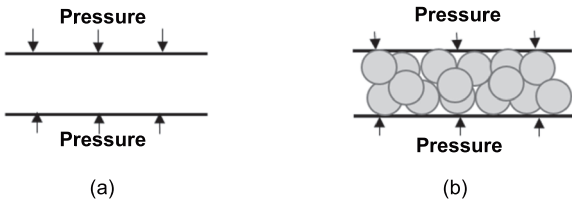

Fig. 1. Fracture opening a) unpropped and b) propped.

mD or higher than 20 mD are usually not treated [7]. Furthermore, the magnitude of the ambient effective stress is an essential factor to be considered [8,9]. This is because several studies, especially those in deeper reservoirs show that with the increase in effective stress, the newly developed fractures rapidly close following stimulation, staunching the recovery of gas. This potential issue may be countered by the injection of proppants with the fracturing fluids – to prop the fracture open. This forms a narrow pathway for the gas to flow to the wellbore. Coal seams occur at a broad spectrum of depths – from shallow to very deep – a few hundred meters to several kilometres from the surface [7,10]. For seams close to the surface, the use of proppants may not be that influential, compared to greater depths [10–12]. Therefore, hydraulic fracturing in coal seam reservoirs can be implemented in two different modalities; 1) injection of pure fracturing fluid and 2) injection of fluids mixed with proppants [13].

Thus, a key question arises in defining suitable criteria, 'when is proppant based hydraulic fracturing effective in coal seam reservoir development?' Limited observations in field and laboratory studies give some insight into this. Field tests at the Soldier Canyon Coal Mine, in Utah [14] propped five hydraulic fractures along a 2505 foot - long horizontal borehole. These showed a 46% increase in gas production over a three week period relative to the unpropped hydraulic fractures. A similar positive result was observed at the Dartbrook coal mine [15], where sand propped fractures increased recovery by a factor of 5. Comparable outcomes to the field test results were apparent in controlled laboratory experiments for He and CO_2 injected coal fractures [16], where the CO_2 permeability of the propped fracture in bituminous coal was 1–2 orders of magnitude higher than the unpropped coal fracture. Similarly, the permeability of a bituminous coal sample at constant pore pressure but varied effective stress (1 to 6 MPa) by Wu et al. [6] identified the CH_4 permeability of a propped fracture in the bituminous coal to be 2–3 orders of magnitude higher than the unpropped fracture.

Although such laboratory observations identify the significance in using proppants in coal fractures to enhance fracture conductivity, it is crucial to have a broader understanding of the impact of the specific techniques to answer the questions of when and how to use proppants in CSG reservoirs. For propped and unpropped fractures, the initial phase of the fracturing treatment is quite similar, where a hydraulic fracture is created or an existing fracture is extended due to the influence of the high fluid injection pressure [17]. The injected fracturing fluid fills and drives the fracture in both scenarios – except in one case where the fluid is proppant-laden [18]. This makes essentially no difference in the initial stages of fracture development, and the fracture width in both pure fluid-based and proppant-based hydraulic fracturing is the same if other controlling factors are kept consistent. The major difference in the propped fracturing application is at the initial phase; proppants fills the developed fracture space before the fracture pressure depletion (Fig. 1). The consideration of the initial fracture width in an unpropped and propped fracture is not considered in experimental studies reviewed to date. This gives an unfair advantage to the propped fracture over the unpropped fracture when comparing the fracture conductivity because, as mentioned above, during the fracture creation, the initial fracture width is the same in both cases. The initial fracture width consideration, especially for the unpropped case, allows the fracture to simulate the fracture closure when the fluid pressure is released. This allows a fair comparison of the fracture conductivity between the unpropped and propped fracture because the initial conditions in both cases are kept consistent.

Understandably, proppants' existence can reduce the fracture conductivity depletion during the well shut-in or flow back stage [19]. However, as mentioned before when considering coal seam reservoirs, it is vital to understand whether reservoirs at shallow depths, are actually improved by the presence of proppants. This is because, at shallow depths, due to the low overburden stress, the created fractures may remain open even after the fracture pressure depletion for unpropped fractures. On the other hand, adding proppants merely plugs this otherwise open pore space with a high tortuosity medium, significantly reducing the available pore space and net limiting the fracture conductivity. In this case, the impact of tortuosity may predominate in controlling the fracture flow [20]. Therefore, it is essential to consider shallow coal seams as well as deep coal seams to understand the impact of proppants at different geological depths, which is one of the primary focuses of this study. Besides, proppant embedment is most likely to occur in soft rock formations such as coal due to its low stiffness nature, which could also significantly impact the fracture conductivity.

Coal in Australia has different stiffness ranks ranging from high stiff anthracite/bituminous coal to low stiff brown coal, where the implementation of proppants and the effect of rank on fracture conductivity is necessary to select the apt coal formations for hydraulic fracturing. Congruent with this hypothesis, we investigate the effects of proppant layering and coal maturity on coal fracture permeability using a suite of flow experiments under in situ stress conditions.

We explore the evolution of permeability in both propped and unpropped fractures in coal through a series of permeability experiments under various confining stresses while carefully examining the initial fracture width of the propped and unpropped fracture. We increase the range of confining pressures from 1 to 20 MPa, to cover shallow coal seams of ~ 200 m and deep coal seams of ~ 1800 m. Specific experimental variables are; proppant loading, coal rank and fracture surface morphology. These features were evaluated by experimental results coupled with the micro-CT (XCT) analysis to establish the role of those on proppant embedment or other damage mechanisms and the corresponding impact on the fracture permeability.

2. Theoretical background

2.1. Darcy flow through a hydraulic fracture

Fluid flow through porous media in laminar flow regimes, where the viscous forces are dominant, can be expressed using Darcy's law as follows:

$$-\nabla p = \frac{\mu Q}{kA} \tag{1}$$

where ∇P is the pressure gradient, μ is the viscosity of the flowing fluid flowing through the porous media (Pa•s), k is the permeability of the porous medium (m^2), Q is the discharge (m^3/s), and A is the cross-sectional area (m^2). However, when the fracture is not completely closed, the flow through the fracture is regarded as pipe flow rather than seepage in coal. In such instances, the bottom area of the fracture is considered to calculate the permeability instead of the cross-sectional area of the coal sample. Idealising a hydraulic fracture to two smooth parallel plates with narrow opening, the volumetric flow rate can be expressed by the 'cubic law' defined in Eq. (2) [21]. Similar to the Darcy's law, cubic law is only applicable when the viscous forces are dominant, and the inertial forces are negligible.

$$Q = \frac{we^3 \nabla p}{12\mu} \tag{2}$$

where w is the width of the fracture normal to the flow direction (m) and

e is the fracture aperture (m). Coupling Darcy's law with cubic law, the permeability (k) of a hydraulic fracture is commonly determined according to Eq. (3).

$$k = \frac{e^2}{12} \tag{3}$$

Hydraulic fracture surfaces in reality are rough, oppose to the assumption idealised in 'cubic's law'. Nevertheless, cubic law is widely applied for rough walled fractures, but with aperture **e** being replaced by hydraulic aperture $\mathbf{e_h}$, assuming that the equivalent hydraulic aperture $\mathbf{e_h}$ exhibits the same fluid flowing capacity as the original rough walled fracture [22].

2.2. Non- Darcy flow through a fracture

When the flow velocity increases, the excessive momentum transfer can perturb the streamlines, developing inertial forces, which could influence the onset of flow transition from Darcy flow to non-Darcy flow. The Forchheimer's equation is generally accepted to have adequately characterize the non-Darcy/non-linear flow through hydraulic fractures.

$$-\nabla p = AQ + BQ^2 \tag{4}$$

A and B coefficients are associated with intrinsic permeability and inertial effect, respectively, in a non-linear flow regime. They are commonly defined as follows for non-linear flow in hydraulic fractures [23].

$$A = \frac{\mu}{kA} = \frac{12\mu}{we_h{}^3} \tag{5}$$

$$B = \frac{\beta\rho}{A_h{}^2} = \frac{\beta\rho}{w^2 e_h{}^2} \tag{6}$$

where β is the non-Darcy coefficient (m^{-1}), and ρ is the fluid density (kg m^{-3}). Note that when the inertial effects are negligible, the Forchheimer's law simplifies to Darcy's law, i.e., $\beta = 0$. Although e_h defined in the Darcy region provides an equivalent hydraulic fracture, yielding the same conductivity as the original rough walled fracture, in non-linear flow, the hydraulic aperture decreases with increased flow rates due to the non-linear effect. This study implements the same approach of Nowamooz, Radilla, Fourar [24] and Fourar, Bories, Lenormand, Persoff [25] used for modelling non-linear flow models, and e_h is regarded as independent from varying flow rates. Determining the onset of flow transition has been a tough ask, and Reynolds number has been the most widely used criterion to determine that. A range of critical values has been published and reported in the literature, making it hard to define a clear boundary to define the onset of non-linear flow transition. A dedicated paper investigating the non-linear flow behaviour through hydraulic fractures has been published by Ranjith, Viete [26]. In their paper, Reynolds numbers up to 4 showed excellent agreement with the non-darcy flow for unpropped fractures, after which the applicability of Darcy's law was questionable. A detailed study by Zhou et al. [25] provided a different approach to identifying the onset of flow transformation. They introduced a critical Reynolds number based on a non-Darcy effect factor (α). For engineering applications, this non-Darcy effect factor (α) is considered as 10%.

3. Methodology

3.1. Coal sample preparation

The present study contrasts the response of bituminous and brown coals from Australia as potential reservoir formations. All samples were acquired as 300 mm × 300 mm × 300 mm block samples, in-mine, and were double-sealed using polyethylene films immediately upon recovery. The coal blocks were preserved in a fog room at the Deep Earth Engineering Laboratory (DEEL) at Monash University until cored. X-ray diffraction (XRD) was used to identify the mineral composition of the two types of coal. The mineral composition of the bituminous coal included 12.3% kaolinite, 3.2% calcite, 2% siderite, 1.5% ankerite, with the remaining comprising organic content. The brown coal comprised principally organic matter with less than 1% comprising mineral matter (quartz, kaolinite and iron sulphides) [27].

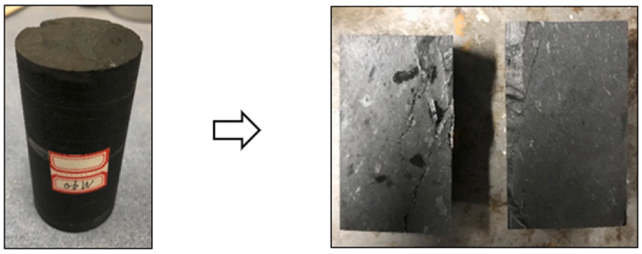

Fig. 2. Cylindrical coal sample split into two cores.

Congruent to ASTM specifications, the coal blocks were cored to 38 mm diameter then cut and ground into 76 mm long cylinders (again at DEEL at Monash University) (Fig. 2). The samples were surface polished to provide smooth and parallel surfaces and then remeasured. The samples were cut longitudinal along their diameter using a diamond saw to produce a relatively smooth artificial fracture (Fig. 2). The fracture surfaces of all samples were smoothed using sandpaper. Finally, the prepared samples were saturated with 10% brine to recreate the salinity conditions experienced in the field. The bituminous coal samples were labelled as A, B and C, and the brown coal D, for a total of 4 samples.

3.2. Proppant preparation

Frac-sand and ceramic proppants were selected as the proppant type for the present study. It is the most prevalent proppant types in the oil/gas industry, and both have reasonably low specific gravity – the latter slowing the settling of the proppants in the injected fluid and allowing longer transport along the fracture [28,29]. We used one of the most common proppant sizes, 20/40# mesh, providing a particle size ranging from 0.425 mm to 0.850 mm. The mineral composition of the proppants was studied using energy dispersive spectroscopy (EDS) (Fig. 3c), identifying a high concentration of silica (SiO_2) in sand, which visually is more evident from the yellowish tinge on the proppant surface, whereas ceramic proppants were high in alumina, which determines the strength of the ceramic proppant. The 20/40# sand and ceramic proppants were saturated with the same injected fluid (water) before the triaxial experiments.

3.3. Experimental apparatus

The permeability experiments were conducted using a high-pressure triaxial apparatus in the DEEL Laboratory at Monash University. The schematic diagram of the apparatus is shown in Fig. 4, comprising a: 1) pressure cell, 2) load frame, 3) fluid pumping system, and 4) data acquisition system. The fluid pumping system comprises two separate pumps to independently apply confining pressure and to inject water along the propped fracture [13,30]. The apparatus can provide a confining pressure of 70 MPa, injection pressure of 50 MPa, axial loads to 100 kN and a maximum temperature 70 ^{0}C. The confining pressure, injection pressure, vertical load and the accumulation of water mass at the fracture outlet was recorded with time throughout the experiment using the data acquisition system.

3.4. Experimental procedure

3.4.1. Triaxial permeability tests

A series of triaxial permeability tests were conducted to understand

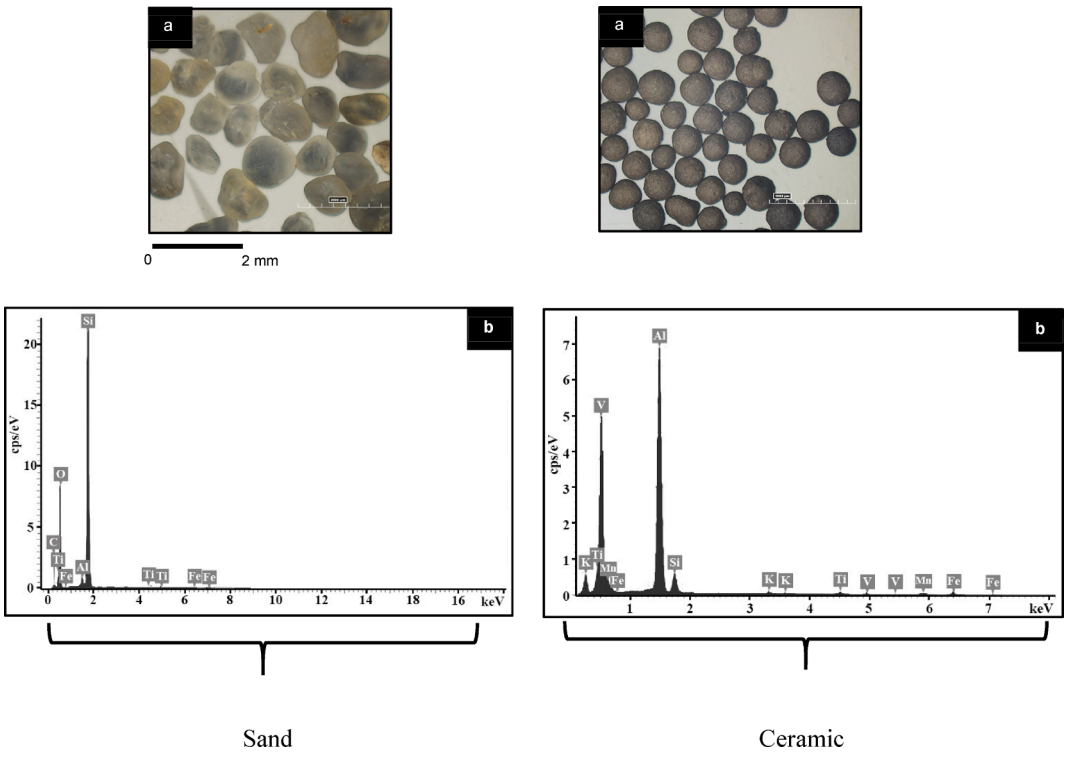

Fig. 3. Visual examination test results. a) Optical microscopy image, b) EDS results.

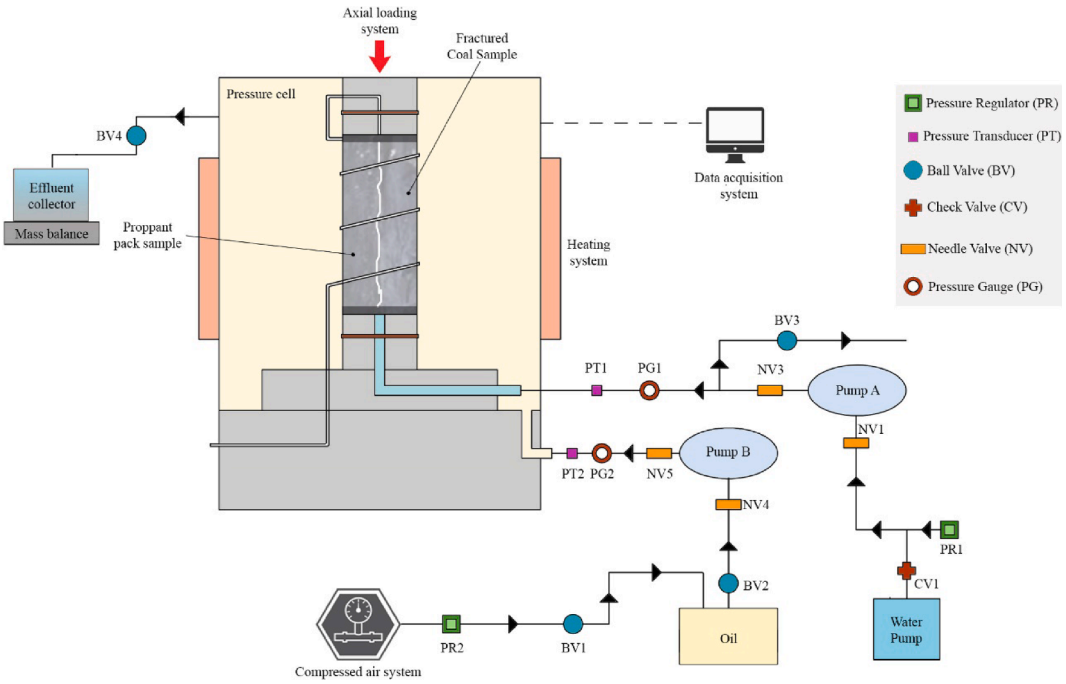

Fig. 4. Schematic of the triaxial apparatus.

the evolution of permeability with stress in propped coal fractures in response to proppant loading, and coal rank. In particular, two direct comparisons were examined:

1. Unpropped vs. propped fracture flow.
2. Impact of coal rank on propped coal fracture flow.

Experiments were conducted under recreated confining stresses, while the axial stress was controlled such that $\sigma_1 = \sigma_3$ (Fig. 5). Appropriate magnitudes of confining stress relevant to typical depths of coal seams [9] (Fig. 6) were selected in the range 1 MPa to 20 MPa, representing seam depths from 400 m to 1800 m. The following subsections explain the procedure for each experimental series.

3.4.1.1. Unpropped vs. Propped fracture flow. Two samples were tested to investigate the proppant loading on coal fracture flow. Each sample

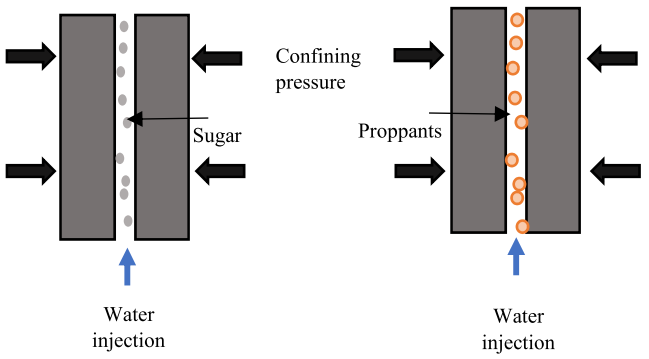

Fig. 5. Simplified schematic diagram of the tri-axial permeability experiment.

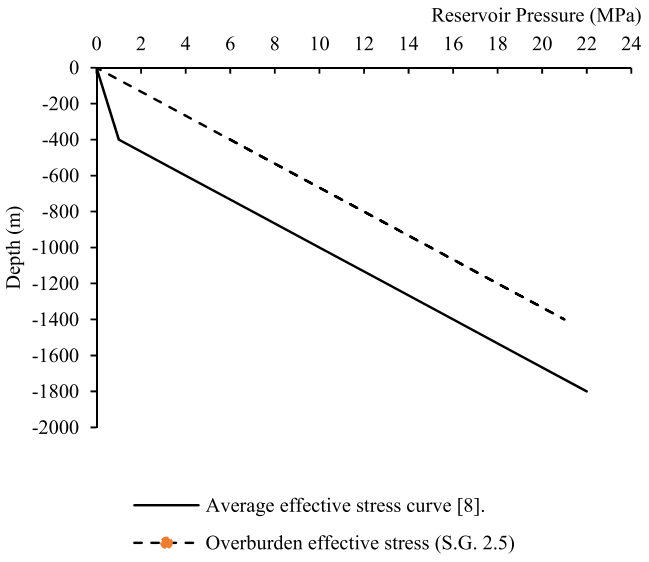

Fig. 6. Correlation between depth and confining pressure relevant for Australian coal seams.

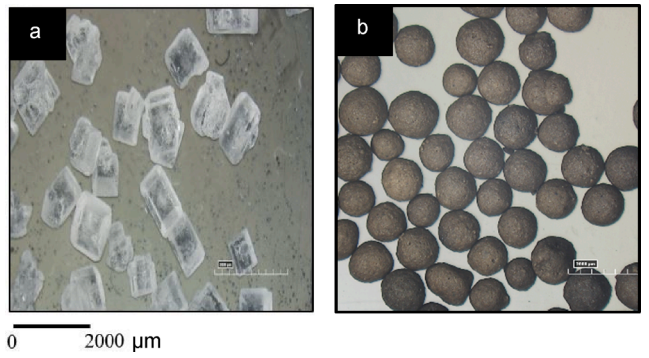

Fig. 7. Comparison between microscopic images of a) Sugar, b) Ceramic particles.

was tested for two different experimental cases conducted in sequence as follows:

Case 1. The sample with saw cut fracture-filled with sugar (unpropped condition- Fig. 8a).

Case 2. The sample with saw cut fracture-filled 20/40# graded ceramic with 20% proppant coverage (propped condition- Fig. 8b).

Case 1 was carried out first. The two halves of the coal sample were

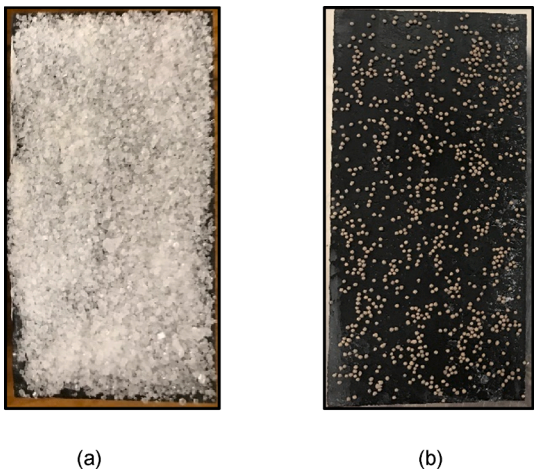

Fig. 8. Experimental cases. a) Case 1- unpropped, b) Case 2 - propped.

taken from the saturation chamber, and sugar was placed on one of the fracture surfaces. The primary reason to place sugar in the unpropped condition is to ensure that the initial fracture width in the unpropped and propped condition is the same. This was executed by first acquiring microscopic images of random samples of sugar and 20/40# ceramic (Fig. 7). The sizes of the sugar particles varied from 225 μm to higher than 1200 μm, but most particle sizes concentrated towards 1000 μm – 1200 μm. The size of ceramic particles varied between 400 μm and 800 μm, which is the standard size variation for graded 20/40# ceramic [31]. This shows that the sugar particles appear to have a larger particle grain size than ceramic. For further reassurance that the initial fracture width in both cases is comparable, both the unpropped and propped sample fracture width was measured using a Vernier calliper before the permeability experiment. However, it must be noted that the sugar particles are a weak link and do not contribute to any resistance. Nevertheless, before the experiment begins, the sugar particles in the fracture needs to be eliminated to simulate an actual fracture. Therefore, before the first reading in the unpropped case was taken, water was injected at 175 kPa pressure at a confining pressure of 1 MPa (which is the first tested confining pressure) to completely dissolve the sugar particles. In order to ensure the sugar syrup formed by the dissolution of sugar particles does not interrupt the flow, the injected water volume was allowed to flow for 140 mL pore volume; approximately more than twice the pore volume required to achieve the steady-state flow rate. It must be noted that the concentration of sugar particles on the fracture surface in the unpropped case does not contribute to the fracture conductivity results since it dissolves and is washed away from the fracture surface with the injected water at the beginning of the test series.

The second coal core was then placed on top of the sugar-filled fracture surface (Fig. 8a), and the intact sample was wrapped with a cling wrap tightly with sticky tape. The intact sample was covered with a specially designed rubber sleeve to avoid the leakage of hydraulic oil into the sample during the application of confining pressure. Porous disks were placed at the top and bottom of the sample with the pedestals before installing into the triaxial rig. In Case 2, instead of sugar, ceramic proppants were placed (Fig. 8b). The reason to choose ceramic proppants is to avoid proppant crushing during the experiment. The proppant coverage used in all propped coal fractures tested is 20%. It must be noted that the proppant coverage of 20% gives a concentration value of 0.292 kg/m^3 for #20/40 ceramic proppants (Case 2) and 0.250 kg/m^3 for #20/40 sand proppants (Case 3), which is derived based on the weight of the proppants used with respect to the fracture surface area. The same proppant distribution in all samples was kept with the aid of 1x1 mm grid mapping on the fracture surface area and by observing the final proppant distribution through optical microscopic images. Past experiences have shown that a proppant coverage of 20% presents a

Table 1
Summary of the samples tested and their experimental conditions.

Sample label	Coal type	Unpropped		Propped		
		Confining pressures (MPa)	Injection pressures (MPa)	Proppant type and coverage	Confining pressures (MPa)	Injection pressures (MPa)
Sample A	Bituminous	2.5, 5, 7.5, 10, 12.5,15	1	–	–	–
Sample B	Bituminous	2–16	0.25	20/40# ceramic with 20% coverage	2–16	0.5,1,1.5,2.0
Sample C	Bituminous	–	–	20/40# sand with 20% coverage	2–10	0.25
Sample D	Brown	–	–	20/40# sand with 20% coverage	2–10	0.25

reasonable fracture width with quality flow data.

In Sample A, water was injected under constant pressure of 1 MPa, and the confining pressures tested for this series was 2.5,5,7.5,10,12.5 and 15 MPa. However, only the unpropped fracture results were obtained; due to leakage and sample failure during the execution of the propped fracture case (Case 2). Sample B was conducted for both cases, Case 1 and Case 2. Initially, for the unpropped case (Case 1), the triaxial permeability test was carried out for a constant injection pressure of 250 kPa under confining pressures ranging from 2 to 20 MPa in 1 MPa increment. However, for the propped case (Case 2), due to high flow rates, the Reynolds numbers were well beyond the critical values given in the literature, which meant the applicability of Darcy's law is questionable. Therefore, under each confining pressure, four injection pressures were tested; 0.5, 1, 1.5, 2 MPa, to adopt the study approach of Nowamooz, Radilla, Fourar [24] and Fourar, Bories, Lenormand, Persoff [25] in determining the permeabilities for non-linear flow models. The permeabilities for the linear flow models were calculated using Darcy law, and the permeabilities for the non-linear flow models were calculated using Forchheimer's law.

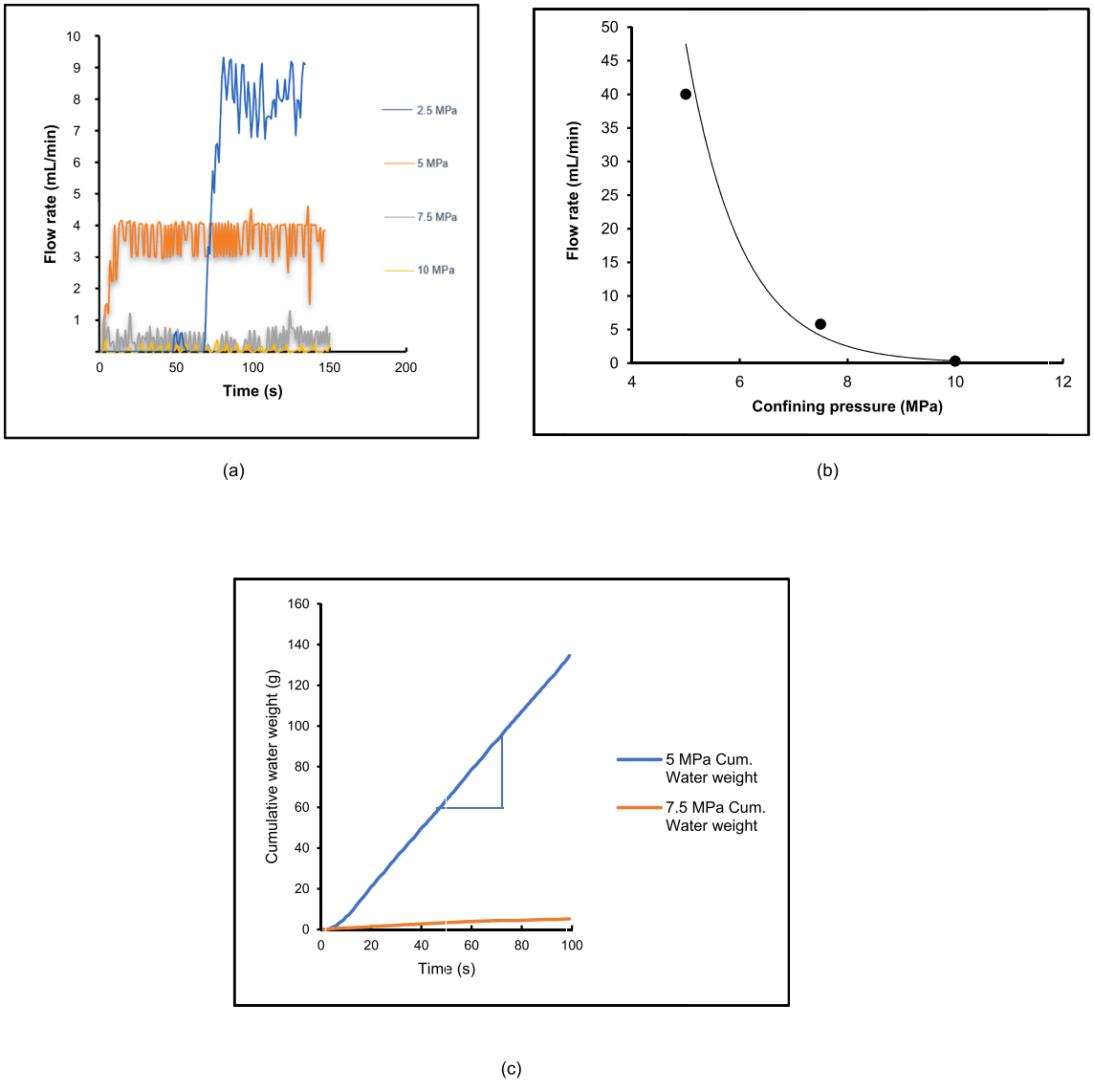

Fig. 9. Unpropped fracture flow rates for sample A for a constant injection pressure of 1 MPa. a) Flow rates variation with pressure, b) Achieved final steady-state flow rate, c) The cumulative water weight with time for confining pressures 5 and 7.5 MPa.

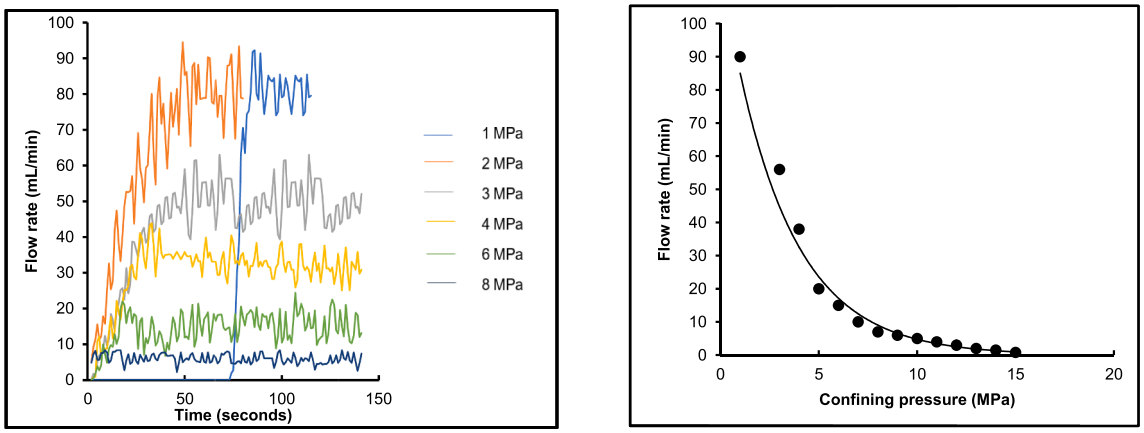

(a) (b)

Fig. 10. Unpropped fracture flow rates for sample B for a constant injection pressure of 0.250 MPa. a) Flow rates variation with pressure, b) Achieved final steady-state flow rate.

3.4.1.2. The impact of coal rank on propped coal fracture flow. Water was injected at a constant pressure of 250 kPa, and the confining pressures tested were from 1 MPa to 10 MPa in 1 MPa increment. Frac sand 20/40# size was selected as the proppant type for this experimental series. Two experimental cases were tested during this experimental series.

Case 3. The **bituminous** sample with a saw cut fracture-filled with 20/40# sand with 20% proppant coverage.

Case 4. The **brown** sample with a saw cut fracture-filled with 20/40# sand with 20% proppant coverage.

The final sample preparation and the experimental procedure was carried out as discussed under Section 3.4.1.1. Table 1 shows the summary of the samples and the test conditions.

3.4.2. X-ray CT measurements

To visualise the surface morphology changes on the fracture surface and possible embedment due to the indentations from the proppants, micro-CT scan (XCT) images were taken for all samples after completing each test. The scanning was conducted at the Australian Synchrotron Imaging and Medical Beamline (IMBL) facility, obtaining 3D reconstructive data at an isometric voxel size of 18 μm. The 3D XCT images were obtained at a resolution of 18 μm by post processing the radiographs by constructing the electrons captured by the special XCT detector. The optimum scanning settings that produced the minimum pixel noise for the images was when the monochromatic beam in mode 3 – Hutch 3B was effectively used at 60 keV energy level to scan the images. At the same time, 1800 projections were taken at multiple angles for each sample with an exposure time of 0.1 sec. The 3-D reconstruction of the XCT images and the analysis of the microstructural features of the images were conducted by post-processing the XCT images using Avizo software.

3.4.2.1. Proppant embedment analysis. 32-bit 3D data were imported and reoriented so that the fracture plane is parallel to the x-y plane. The volume region, which concerns the fracture space, was extracted using the sub-volume extraction tool from the total reconstructed sample volume. The primary objective of the XCT analysis was to segment the indentations from the coal material and find the depth for each indentation. Due to the uneven fracture surface and for the simplification of the analysis, the fracture surface was divided into several sections depending on the topography of the surface (Fig. 17b). Each section was analysed separately, and the embedment was quantified.

The indentations in the fracture surface were segmented using the interactive thresholding tool to develop a binary mask in the grayscale histogram of the XCT data. The segmented indentations were separated using a separate algorithm object. However, the segmentation of indentations was complicated by the indentations having a similar density to the coal material. Therefore, to remove these inclusions and seams within coal, a combination of several segmentation tools such as the brush tool, 2D and 3D lasso tool and magic wand tool was used. Once the high dense material within the segmented mask was removed, within a particular volume range, the threshold of the applied filter was manually adjusted to ensure only proppant indentations were selected in the final segmentation. Finally, to determine the embedment of induvial proppant particles, a label operation was performed on the indentations, which provides the number of indentations for each slice in the z plane. It must be noted that although coal is a porous medium, the pore sizes in coal are generally less than 1 μm [32]. Therefore, the pores within the coal matrix will not be detected in this XCT scan because the samples were scanned at a voxel size of 18 μm, which is directly linked to the pixel size as well as the slice thickness. The indentation widths observed (Fig. 17b) through the topographical view are approximately within the 50–200 μm range, which is well above the range of large coal pores, ensuring the segmented indentations are only from proppant embedments. Furthermore, the accuracy of the embedded depth obtained by the XCT scan is 18 μm.

4. Results

4.1. Triaxial permeability test results

4.1.1. Unpropped vs. Propped fracture flow

The triaxial test results comparing the permeability of an unpropped vs. propped fracture with pressure is illustrated in this section. As mentioned in section 3.4, sample A was tested only for the unpropped condition, while sample B was tested for both unpropped and propped conditions. Sample A unpropped flow rate plots are shown in Fig. 9, and Sample B unpropped flow rate plots are shown in Fig. 10. The final steady-state flow rates were taken from the slope of the graph plotted between cumulative water weight and time. An example of the plot between the cumulative water weight and time for sample A at 5 and 7.5 MPa confining pressure at an injection pressure of 1 MPa in the unpropped condition is shown in Fig. 9c. In both samples, the time taken to achieve the flow rate is always higher for the first permeability test (i.e. 2.5 MPa for sample A and 1 MPa for sample B) compared to the rest of the subsequent tests. The delay is associated with the time taken for the dissolution of sugar particles. The results also show that until 5 MPa, although the degree of flow reduction is higher, the flow in the

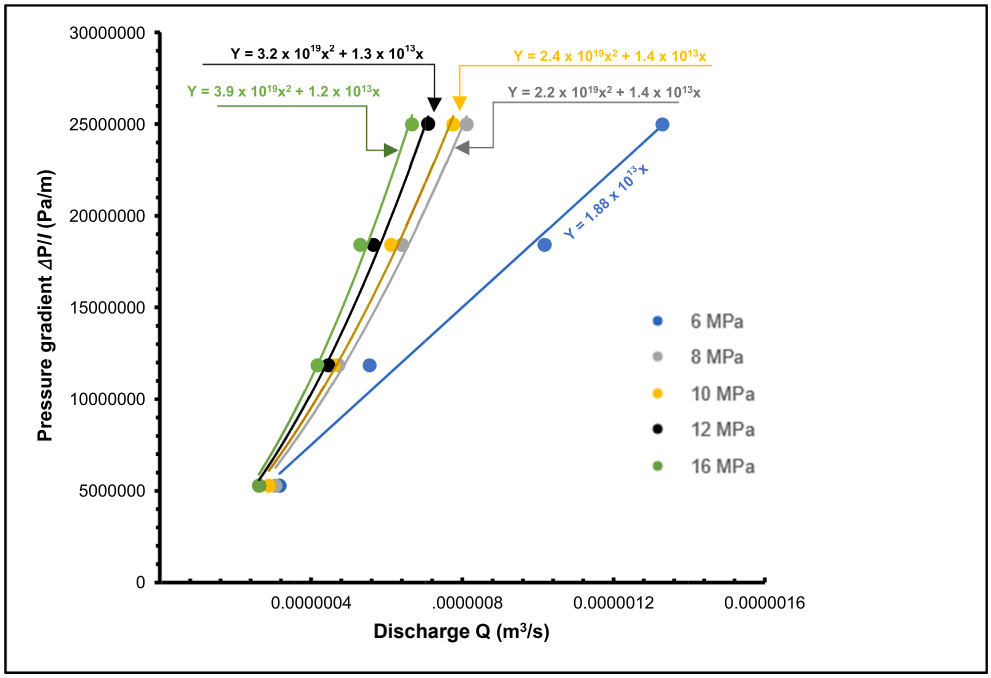

Fig. 11. Best-fit curves obtained for the propped coal sample (Case 1) for selected confining pressures.

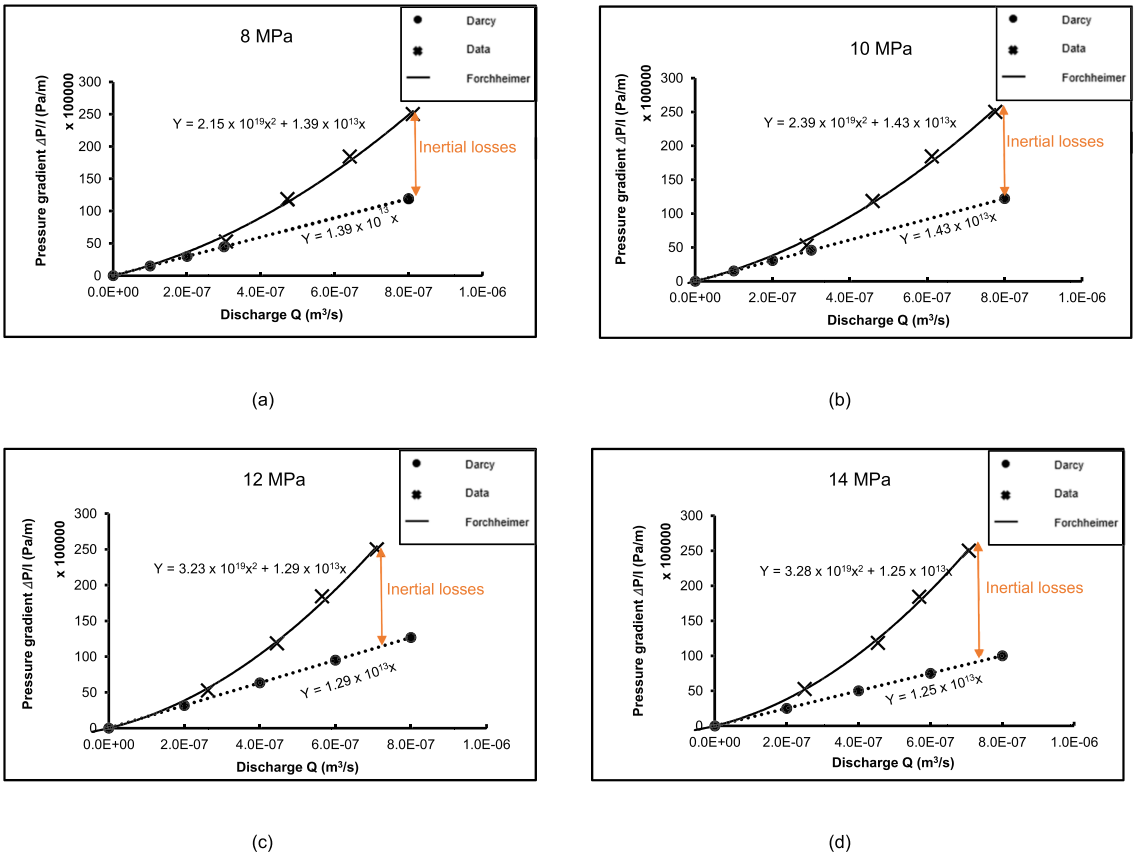

Fig. 12. Individual flow plots for the propped coal sample for selected confining pressures.

unpropped fracture is above 20 mL/min, which is reasonably high conductivity. Beyond 5 MPa, the fracture flow reduction is gradual and eventually, the flow becomes slender, overall exhibiting an exponential flow reduction with pressure. The permeabilities for the unpropped fracture were calculated using Darcy's equation [Eq. (3)]. However, since the flow rates were high until a confining pressure of 5 MPa, the Reynolds number values surpassed the critical values given in literature (Re > 4). Hence, the permeabilities were calculated only for the flow

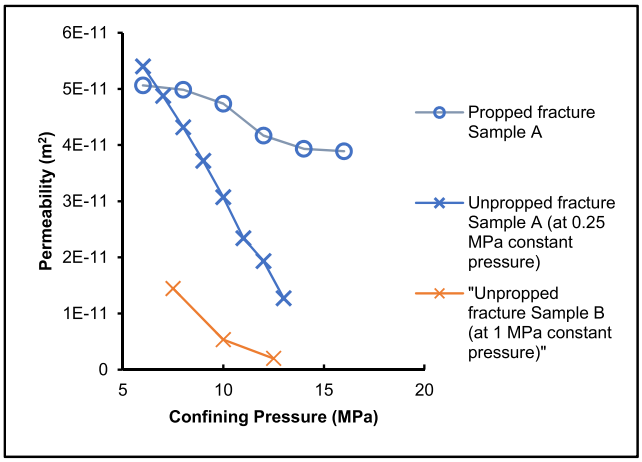

Fig. 13. Permeabilities of the unpropped (Case 1) and propped fractures (Case 2).

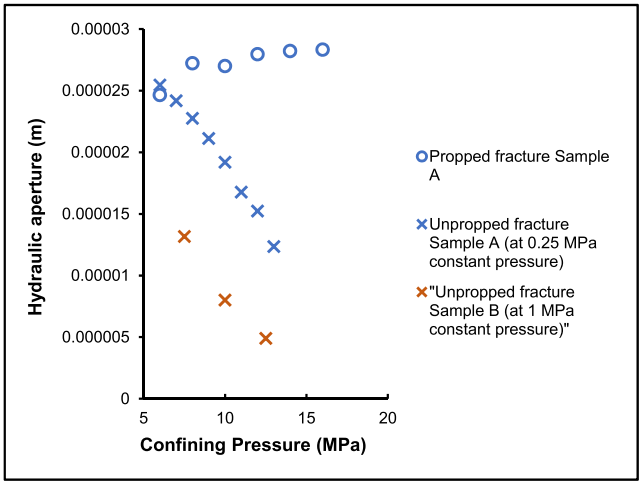

Fig. 14. Hydraulic aperture variation of the unpropped (Case 1) and propped fractures (Case 2).

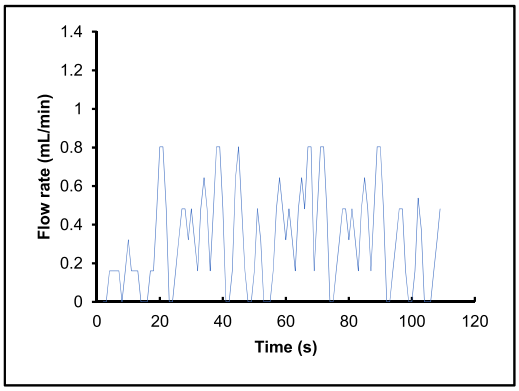

(a)

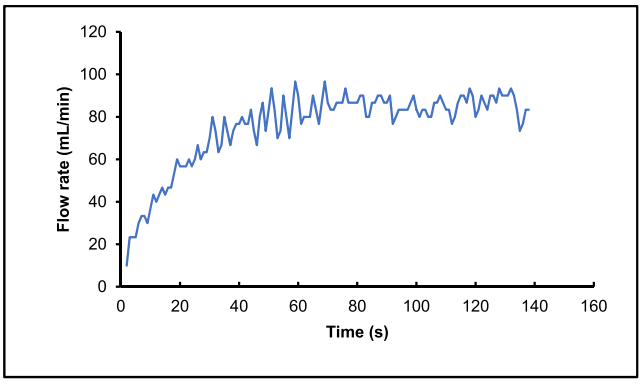

(b)

Fig. 15. Flow rate variation with time under 2 MPa confining pressure and an injection pressure of 0.250 MPa. a) sand propped brown coal sample (Case 4), b) sand propped bituminous coal sample.

data obtained above 5 MPa confining pressure, where Darcy's equation is valid. The corresponding permeability plots for the unpropped condition for both samples are illustrated in Fig. 13.

Sample B was tested for the propped condition with a ceramic proppant coverage of 20%. Since the Reynolds number values for this data were well above the critical limits provided in the literature, the Forchheimier non-linear flow models were adopted. Fig. 11 shows the best-fit curves for the flow data plotted between the pressure gradient ($\Delta P/l$) and discharge (Q). Interestingly, although the Reynolds number values were high, the flow data at 6 MPa was best fitted to the linear Darcy line. The rest of the plots were in excellent agreement with the zero-intercept polynomial function introduced by Forchheimer. The comparison between the linear and polynomial relationship of these plots are further illustrated in Appendix A, Figs. A1–A4. The main noticeable variation in the plots is that the degree of non-linearity increases with pressure, meaning the inertial forces gain dominance over viscous forces with pressure. This is evident in the individual plots in Fig. 12 at selected confining pressures. The Darcy linear line is plotted to identify the point when the flow trendline differs from the Darcy linear relationship. The linear Darcy trendline is plotted based on the linear part of the quadratic polynomial equation. The equation corresponding to each Darcy line is included in the figures given Fig. 12, which indicates it corresponds to the linear function of the quadratic equation.

The permeability for sample B at propped condition was calculated considering the behaviour and is plotted in Fig. 13 along with the permeabilities of sample B at unpropped condition. Comparing the permeabilities for Sample B for unpropped and propped coal fracture, interestingly at 6 MPa, the permeability is higher in the unpropped fracture than the propped fracture. However, beyond the 6 MPa, the permeability values of the propped fracture is higher, and the degree of superiority in permeability over the unpropped fracture increases with confining pressure. Fig. 14 shows the hydraulic aperture variation for the unpropped condition in Sample A and hydraulic aperture variation for the propped and unpropped condition in sample B. The hydraulic aperture is determined from the flow test results assuming that the fracture is idealised as two parallel plates. Therefore, the hydraulic aperture calculated is a function of the flow test results, which depends on the available void spaces between the fracture surfaces. Considering an unpropped fracture, with the increase in confining pressure, the asperities in the fracture surfaces progressively contact and gradually reduce the allowable void space in the fracture. As a result, the flow reduces, and consequently, the hydraulic aperture reduces with confining pressure, as shown in Fig. 14 for the unpropped condition for sample A and B.

In the case of propped fracture, the hydraulic aperture seemed to be consistent and does not show any major reduction with pressure. This is primarily because the presence of proppants does not allow fracture closure similar to the unpropped fracture. However, there seems to be a

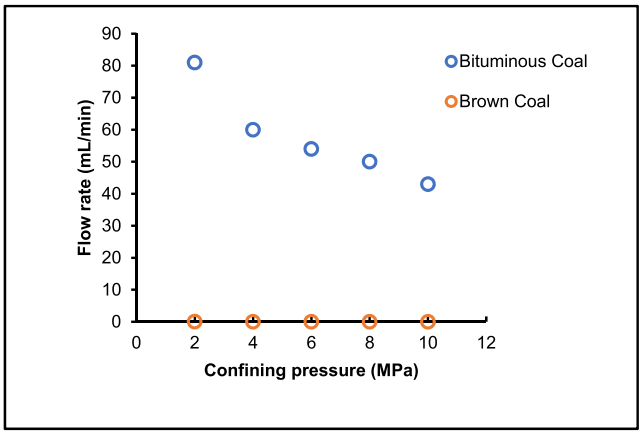

Fig. 16. Achieved final steady-state flow rate for propped bituminous and brown coal sample.

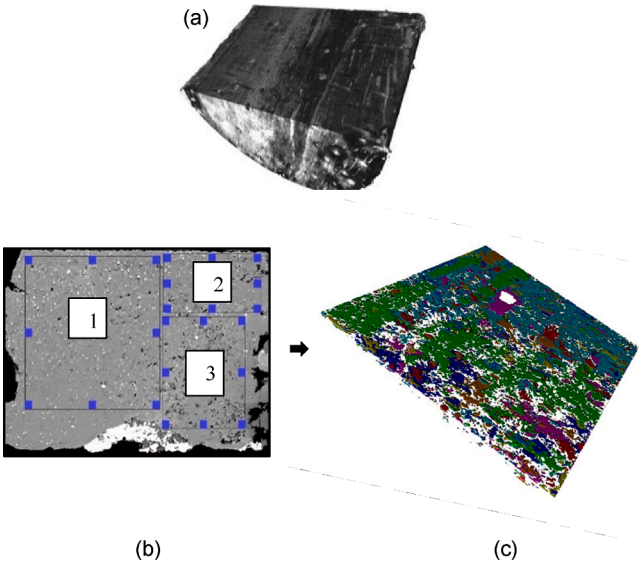

Fig. 17. a) 3D reconstructed coal core, b) XCT image with labels for analysis, c) labelled indentations on the fracture surface according to the indentation depths.

slight increase in the hydraulic aperture for the propped condition in sample B for certain confining pressure transitions (Fig. 14). It must be re-emphasized that the hydraulic aperture is measured based on the flow test results and the curve fitting of the flow data in the Darcy and non-Darcy laws. Unlike in the unpropped fracture, in a propped fracture, the proppants does not allow asperity contact between fracture surfaces unless the degree of proppant damage is high [13]. However, the presence of proppants can obstruct the flow path, inducing tortuosity along the fracture path [33,34]. The degree of tortuosity changes when the confining pressure changes because the smooth surface of the ceramic proppants allows the proppant particles to mobilise in the fracture [35]. The movement of the proppant particles can increase the degree of obstruction or could potentially reduce the obstruction by reducing the flow distance of the fluid in the fracture. The shortening of the flow distance could transpire to the flow results and thereby show a slight increase in the hydraulic aperture, although, in reality, the physical fracture width would have reduced with confining pressure. That being said, the hydraulic aperture is derived for smooth parallel fracture surfaces, and when non-linear flow models are implemented for comparatively large fractures with proppants, it is generally expected to be constant with minor deviations.

4.1.2. *The impact of coal rank on propped coal fracture flow*

Fig. 15a shows the only flow rate achieved by the propped brown coal sample at a confining pressure of 2 MPa and injection pressure of 250 kPa (For comparison, Fig. 15b presents the flow rate variation of the propped bituminous coal sample at the same confining pressure and injection pressure tested). In contrast, the propped bituminous coal sample gave a significant flow rate for all confining pressures. The comparison of the achieved steady-state flow rates with confining pressure for both fracture conditions is shown in Fig. 16 The only difference between the two cases was the coal type.

4.2. *X-ray CT results*

The XCT scans enabled us to analyse the changes in the fracture surface and predict its impact on fracture permeability under different pressure regimes. The high-resolution XCT images obtained from the synchrotron facility were analysed through the access of a supercomputer at Monash University using software tools such as Avizo and Image J (see Section 3.4.2). A 3D reconstructed half core coal sample is shown in Fig. 17a. The 3D reconstructed sample was analysed and segmented using advanced imaging tools. The indentations were segmented according to the indentation depths, and an example of a segmented image of sample C is labelled and shown in Fig. 17c. The different colours in the segmented image correspond to the indentation depths. Figs. 18 and 19 shows the number of indentations under each indentation depth for sample B and C, respectively. The extract number plots in the Figures are the extracted topographical volumes of the surfaces based on the terrain along the fracture. Figs. 18 and 19 show that the embedment depth on the fracture surface is concentrated mostly at shallow depths and decreases rapidly, approaching higher embedment depths. This trend is common to all four fracture surfaces.

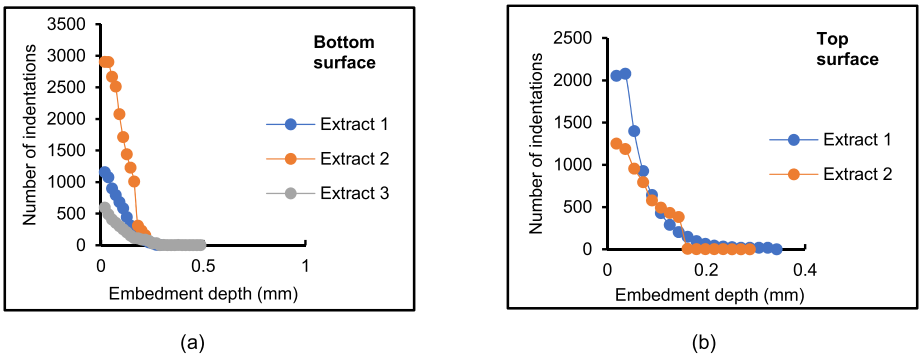

Fig. 18. Number of indentations vs. embedment depth for **Sample B.**

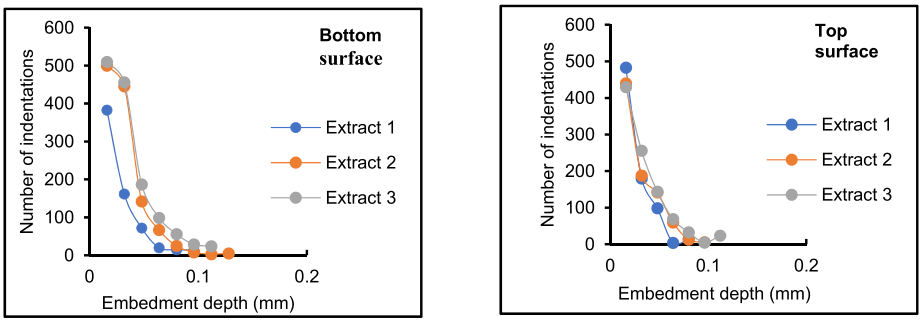

Fig. 19. Number of indentations vs. embedment depth for **Sample C.**

5. Discussion

Series of laboratory experiments were carried out to investigate the fracture flow in coal due to the impact of proppant loading and coal rank. In this section, the above key factors and their influence on fracture conductivity are discussed in detail.

5.1. *The impact of proppants on fracture conductivity in coal*

Fracture permeabilities of bituminous coal samples with propped and unpropped fractures were tested and compared to understand the impact of proppants on fracture flow behaviour in coal. The results are shown in Fig. 13. According to the figure, the permeabilities at unpropped condition for both samples A and B gradually reduced with the increasing confining pressure. Interestingly, comparing the unpropped fracture permeabilities, the unpropped fracture permeability in sample B at an injection pressure of 1 MPa is lower than the unpropped fracture permeability obtained for sample A at an injection pressure of 250 kPa under the same confining pressures. This result contradicts with the well-known fact that the permeability is inherent and independent of the injection pressure. Having said that, the mechanism of permeability reduction in unpropped fractures is through the progressive asperity contact with confining pressure [36], which clearly depends on the nature of the fracture surface (refer Fig. 21). The bituminous coal samples A and B were taken from the same block, and during the sample preparation stage, we aimed to get smooth parallel fractures and thus the asperities of the samples were removed, expecting the coal fracture to close like parallel plates. However, due to the heterogeneity of the coal structure, the sample physical properties in general, and specifically the nature of the fracture surface could differ from sample to sample. The difference in fracture surfaces influences the asperity contact during closure of fracture surfaces, and thereby influence the roughness of the fracture at a given stage [37,38]. This could influence the flow behaviour in the fracture and perhaps the reason for the permeability differences observed for sample A and sample B at unpropped condition.

Furthermore, the fracture roughness is not a constant value during the confining pressure application, rather depending on the fracture morphology, the fracture surface roughness changes along the fracture, influencing the flow behaviour. The permeabilities in Fig. 13 and flow rates in Figs. 9 and 10 for the unpropped condition for sample A and B clearly show that the flow conductivity is different with confining pressure. In the case of sample A, Fig. 9 shows that the degree of reduction in flow is very high with pressure, and more so when the pressure is increased from 5 to 7.5 MPa, where the flow reduced by 90%. This can be attributed to the sudden increase in fracture roughness, which perhaps is expected to occur when both fracture coal surfaces come into contact simultaneously [39]. However, in sample B, the permeability and flow reduction is gradual, and the increase of stiffness

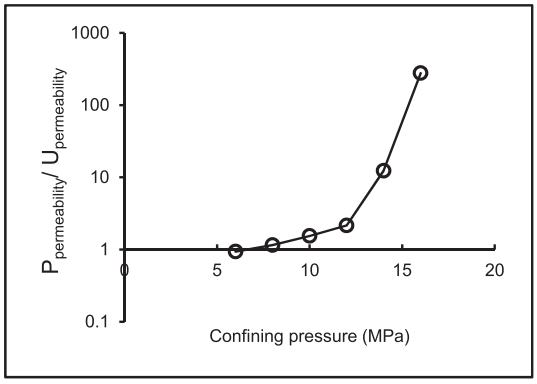

Fig. 20. Correlation between P_{perm}/UP_{perm} with confining pressure (P_{perm} – permeability of the propped fracture, UP_{perm} – permeability of the unpropped fracture).

of the fracture also can be concluded gradual, where the asperity contact is expected to be progressive.

On the contrary, in the propped condition in sample B, the proppants resist the complete fracture closure and therefore, the flow through the fracture is comparatively less interrupted by the fracture roughness caused by the asperity contact. For this reason, as shown in Fig. 13, the permeability does not reduce to the degree observed in the unpropped condition and allows high flow conductivity through the fracture. That said, the presence of proppants in fracture space are bound to develop a resistance to the fracture flow [34]. Interestingly, according to Fig. 13, sample B at unpropped condition shows a greater permeability than for the propped condition at 6 MPa confining pressure. As mentioned before, the flow in an unpropped fracture is determined by its open and closed portion of the fracture, which is dependant on the nature of the fracture surface (refer Fig. 21). At 6 MPa confining pressure, the open portion of the fracture is sufficient to allow a higher permeability than the fracture filled with ceramic proppants. This shows that the propped fractures may not always deliver the oil/gas productivity required, especially for shallow coal seams. According to our results, proppants do not positively impact the fracture flow up to 6 MPa confining pressure,

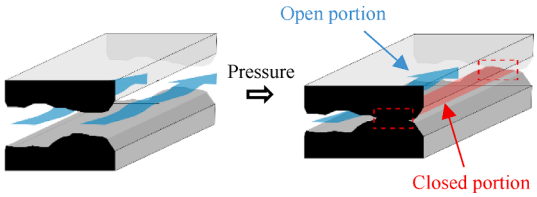

Fig. 21. Open and closed portion of a fracture during the asperity contact.

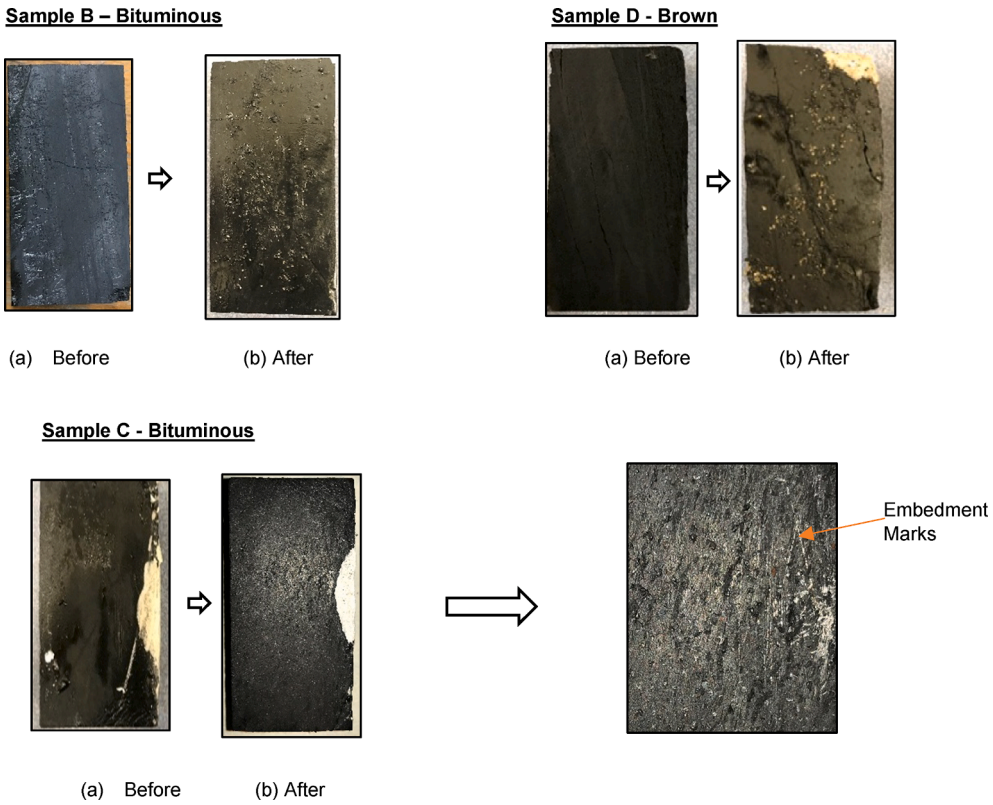

Fig. 22. Fracture surface changes observed after each test series for samples B, C and D.

representing about 700 m depth from the ground surface. This is critical in terms of the requirement of proppants for oil/gas production because a cost breakdown of the stimulation in a hydraulic fracturing treatment presented by Cheung, Hilling, Brierley [39] showed that proppants lead the primary cost involved in a proppant based hydraulic fracturing treatment, and the above information could lead as a cost reduction strategy. Therefore, the proppant based fracturing treatment needs to reap significant economic benefit to achieve economical production from the fracturing treatment.

Fig. 20 shows the propped (P_{perm}) to unpropped (UP_{perm}) fracture permeability ratio variation with the confining pressure. The graph is plotted under a logarithmic scale to illustrate better the variation of permeability ratios. As shown in the figure, the positive impacts of proppants on fracture permeability are greater at higher confining pressure, representing greater reservoir depths. The impact is much more significant when the confining pressure is beyond 10 MPa, where the propped fracture permeability is around 1–2 orders higher compared to the unpropped fracture permeability. This shows that for proppants to be effective, the reservoir pressure needs to be higher than 10 MPa, representing around 1000 m reservoir depth for coal seam gas reservoir formations of similar characteristics. In this study, we used ceramic proppants to investigate fracture flow behaviour. One of our previous studies on proppant damage mechanisms in a propped coal fracture Ahamed, Perera, Black, Matthai, Ranjith, Dong-yin, Sampath [40] shows that sand proppants provide a higher permeability increment in coal than ceramic proppants for shallow reservoirs. However, the results in this paper clearly shows that for shallow reservoirs, the placement of proppants may not be beneficial; and in fact, as Khanna, Keshavarz, Mobbs, Davis, Bedrikovetsky [34] said the additional effect of tortuosity can interrupt the flow path along the fracture [33], reducing the productivity of oil/gas production.

Although the proppants might be very beneficial after a certain threshold stress region, proppant damage has been commonly reported in hydraulic fracturing at such deep coal seam gas reservoirs. The type of proppant damage mechanisms expected in a coal seam gas reservoir is different from other deeper reservoirs due to the heterogeneity and complex material structure of coal [13]. Several theoretical and experimental studies on rock mechanics infer that the low stiffness nature in the coal material makes the coal hydraulic fracture most vulnerable to proppant embedment [41,42]. This was examined by observing coal fracture surface before and after fracture permeability tests for brown coal and black coal and is shown in Fig. 22. The noticeable difference in the fracture surfaces' appearances is the proppant embedment that had occurred on the surfaces, which is different depending on the coal rank. Embedment in soft rock formations can reduce the fracture aperture by 10–60% [43], which decreases the gas production significantly as the fracture conductivity is directly related to the fracture aperture. Therefore, embedment can be a serious problem for production enhancement in gas reservoirs, and to date, there have been very limited experimental studies that quantify embedment on propped coal fractures. Introducing a method to quantify the embedment properly would undoubtedly help understand the impact of embedment on gas production over time.

The quantification of proppant embedment was carried out as discussed under Section 3.4.2.1. The results of the embedment frequencies with depth for bituminous sample B is provided in Fig. 18. The statistical analysis of the data shows that the embedment depth is approximately 0.145 mm. This is interesting in comparison with the embedment depth of 0.060 mm obtained for bituminous sample C, where the fracture was propped with sand proppants. The higher elastic modulus in ceramic proppants allows higher embedment on the coal fracture surface, which in this case was 60% higher than the embedment created by sand proppants. Although the embedment results on the tested samples provide reasonable evaluation, to comprehensively understand the embedment in coal seams, repeating embedment measurements on different coal samples and further evaluating the effect of key parameters on a larger scale is required.

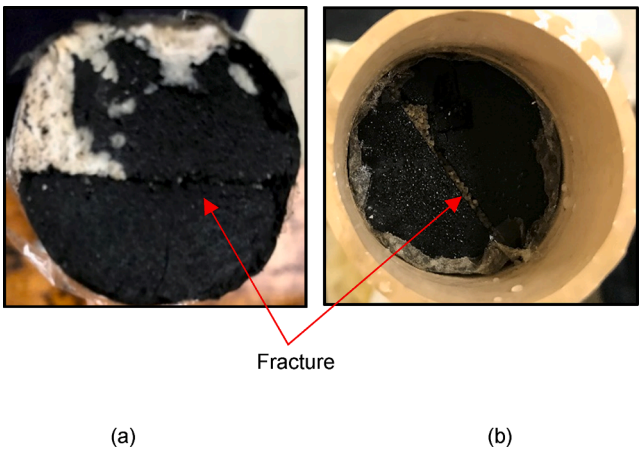

Fig. 23. Tested samples. a) Sample C (Brown coal), b) Sample B (Bituminous coal).

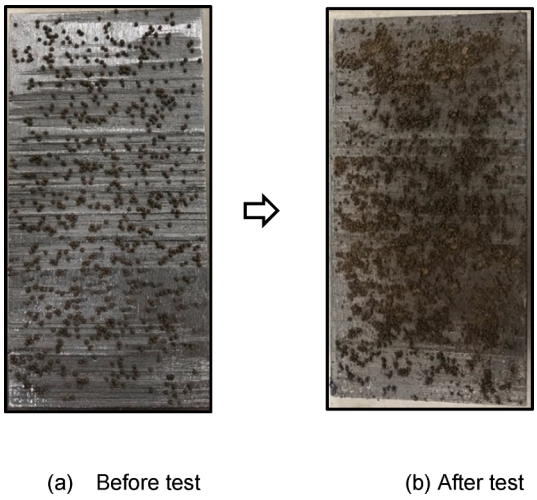

Fig. 24. Fracture surface changes on a steel fracture propped with high strength ceramic proppants at confining pressure of 4 MPa.

5.2. *The impact of coal maturity on proppants performance*

Understandably, proppants damage mechanisms and compressibility of coal matrix with the applied stress depend on the stiffness of the coal mass, which depends on its rank or maturity. The impact of coal maturity or rank on proppant effectiveness was considered at the next stage using bituminous and brown coals, and the flow results are shown in Fig. 16. Here, instead of ceramic, frac sand was selected as the proppant type since preliminary tests showed that the large difference in elastic modulus between ceramic and brown coal induces damage to the sample, causing sample failure during the execution of the experiment. As shown in Fig. 16, the sand proppant layer in the propped bituminous coal sample (Case 3) has the ability to keep open the fracture under greater confining pressures, which is not the case for low ranked brown coal; where the propped brown coal sample shows a minimal flow rate of 0.3 mL/min only at 2 MPa confining pressure and increasing to 4 MPa confining pressure, the fracture flow terminates. The possible reason is the complete fracture closure occurred in the propped brown coal sample, which was evidenced by the appearance of fracture surfaces of the brown coal sample after the testing and is shown in Fig. 23. The two halves of the brown coal sample had merged entirely, completely closing the fracture even after releasing the confinement, which can only occur with 100% embedment of the proppant particles.

This complies with some of the recent theoretical work presented by

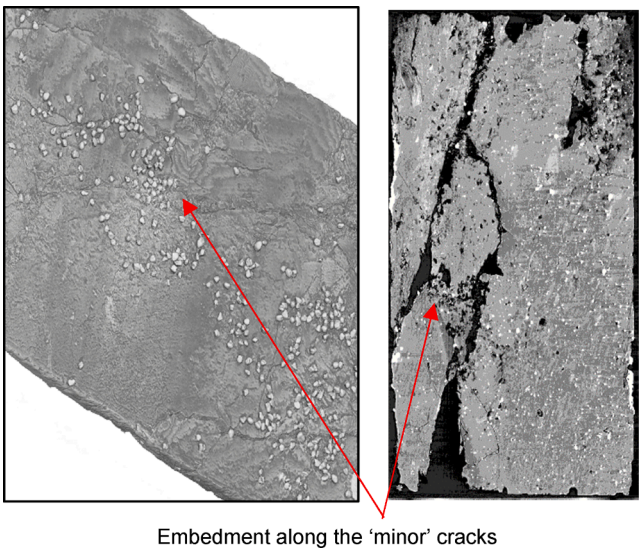

Fig. 25. XCT image of bituminous coal sample (Sample C); embedment along the low to high rough regions.

Li, Gao, Lyu, Wang [41] and Chen et al. [42], where they showed the direct impact of rock mass stiffness on proppant embedment. Similar conclusions have been drawn by Akrad, Miskimins, Prasad [44] based on an experimental study, where the proppant embedment was low for stiff shale samples but for softer shale samples with an elastic modulus less than 6.89 GPa, the proppant embedment systematically increased. Therefore, considering that the proppant elastic modulus is generally higher than the elastic modulus of coal, coal with higher stiffness is more suited for coal seam gas extraction during proppant based hydraulic fracturing. However, when the coal material is very strong such as high-ranked anthracite coal, the selection of proppants could be very critical. Using low strength proppants such as frac sand in high stiff coal, could

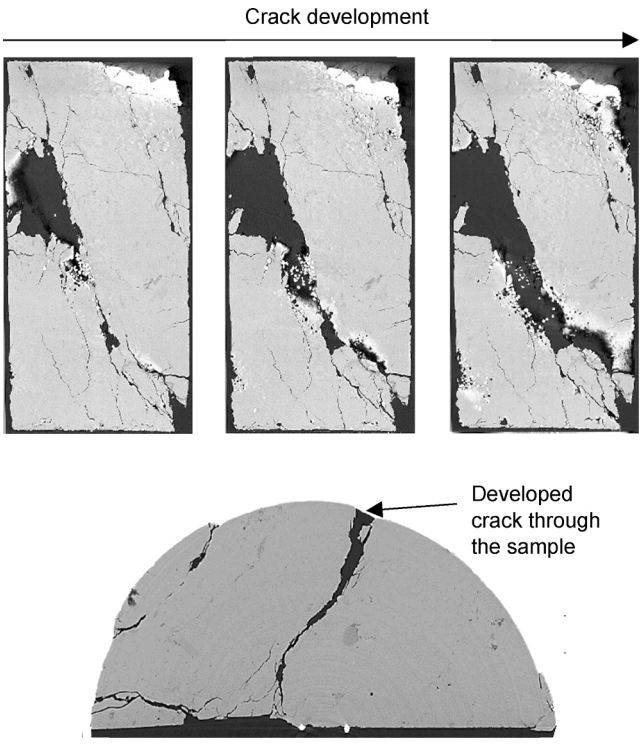

Fig. 26. Image series of the propped brown coal sample (sample D) at the fracture surface illustrating the crack propagation.

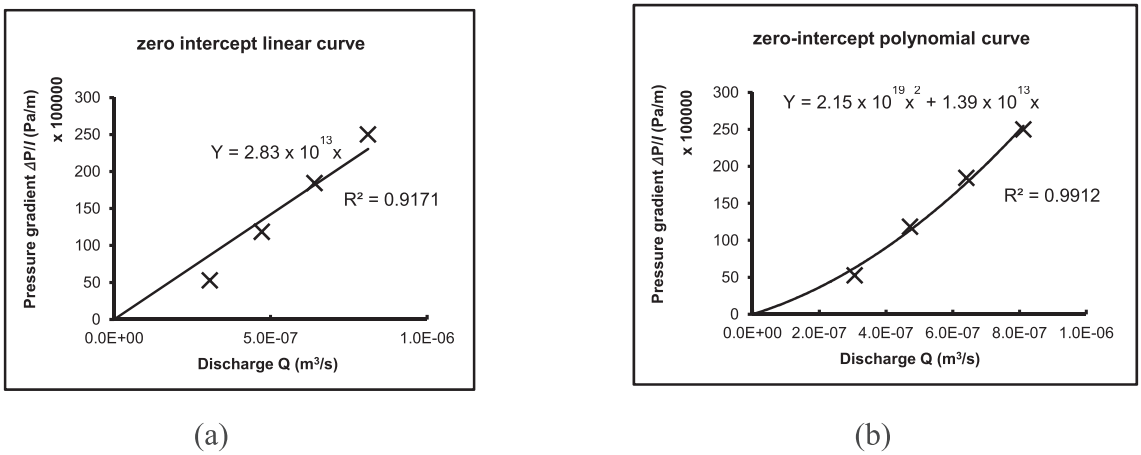

(a) (b)

Fig. A1. Best fit Flow plots at 8 MPa confining pressure for the propped bituminous coal sample. a) zero-intercept linear curve, b) zero-intercept polynomial curve.

change the prone damage mechanism to proppant crushing from proppant embedment. We investigated this by evaluating the flow conductivity of a steel fracture of similar dimensions to the tested coal fracture, propped by high strength ceramic proppants with 20% proppant coverage. At 4 MPa confining pressure, the fracture completely closed with flow not being recorded, exhibiting a complete closure of the fracture. The sample was carefully taken out from the triaxial rig, and upon investigation of the fracture surface, it revealed that the high strength proppants were completely crushed (Fig. 24). This clearly shows that the difference in the proppants and coal's elastic modulus is the key element that requires consideration than the individual stiffnesses of each contact surface before the fracturing treatment.

The embedment of proppant particles along the fracture surface in all the tested coal samples was non-uniform due to the redistribution of proppants caused by the water injection. Such non-uniform distribution of proppants in hydraulic fracture surfaces is highly expectable during the coal seam gas extraction process. The injected water causes the proppant particles to move into certain regions on the fracture surface and form deposition layers by combining with incoming proppant particles [42]. This movement of proppant particles in a fracture also depends on the fracture surface roughness. As the fracture closes with pressure and the fracture surfaces begin to contact the asperities, the fracture surface roughness increases; higher the asperity contact, higher the surface roughness. Therefore, at regions where the surface roughness is high, due to the resistivity, the fluid velocity decreases and becomes quite small, and the particle movement and accumulation is expected to be less [44]. In contrast, at surfaces with lower roughness, the fluid velocity is higher and allows a higher probability of particle movement [44]. These proppant particles usually accumulate in the high to low rough boundaries. The 'minor cracks' (Figs. 25 and 26) within a fracture surface is a good indication to spot the high to low surface rough boundaries [42].

Fig. 25 shows an XCT scanned image of the surface of the bituminous coal sample B, and Fig. 26 is an XCT image series of continuous adjacent slices of the propped brown coal sample C fracture surface. The XCT images show that numerous 'minor cracks' are developed on both fracture surfaces. The above-claimed effect of particle accumulation at the 'minor cracks' is evidenced in the scanned images, where the embedded "pock" marks induced by the proppants are mostly accumulated close to the 'minor crack' region, indicating the high to low surface rough boundaries. This is very similar to the findings of Akrad et al. [42], where they investigated the embedment of proppants for shale rocks. Based on the observations, they concluded that the embedment is most severe at the high- low rough boundaries. According to Akrad et al. [42], the reason for the development of 'minor cracks is because as the pressure is applied on the rock, the region with low roughness allows the proppants to get embedded while stresses build up in the higher roughness region. As a result, this roughness transition zone causes these cracks to develop and thus allow embedded proppants to be concentrated in this region. In some cases the developed minor cracks can lead to major crack propagation along the rock reducing the overall strength of the rock, which was observed in the propped brown coal sample (Fig. 26).

The results are based upon experimentally investigating bituminous and brown coal samples. Due to the contrasting chemical and physical characteristics of brown and bituminous coal, it allows to predict the proppant behaviour in other coal ranks such as anthracite and subbituminous coal as well. However, to draw concrete conclusions, a larger range of coal rank samples should be included in future experimental research studies.

6. Conclusions

The fracture flow behaviour was investigated in fractured coal samples with the injection of water under controlled laboratory conditions. This study investigated the impact of proppant loading and the coal type in coal fracture flow. Based on the experimental results, the following conclusions could be drawn;

- The impact of proppants appears to be effective on coal fractures only after a threshold pressure range of 6 to 8 MPa, which is correlated to a coal seam depth between 700 m and 900 m. For deep coal seams (>10 MPa), the propped fracture permeabilities can be one or two orders of magnitude higher than the unpropped fracture permeabilities.
- Proppants' effectiveness in the hydraulic fracturing process depends on the coal mass's maturity or rank due to the direct impact of coal mass stiffness on the proppant damage mechanisms and the transport process. According to the experimental results, low stiff coals promote proppant embedment, while high stiff coal samples could encourage proppant crushing with the overburden stress.
- Proppants in a hydraulic fracture is prone to accumulate at the boundaries of low to high surface rough regions, causing a greater embedment in these regions while having the potential of instigating major crack propagation within the formation.

This study compares the permeability of unpropped fractures with propped fractures and also compares the impact of coal maturity on fracture conductivity by using the artificial crack to simulate the fracture. Realistically, this is not the ideal condition to create a hydraulic fracture. However, permeability experiments in this version of a fracture, enables to have a controlled experimental environment and isolate

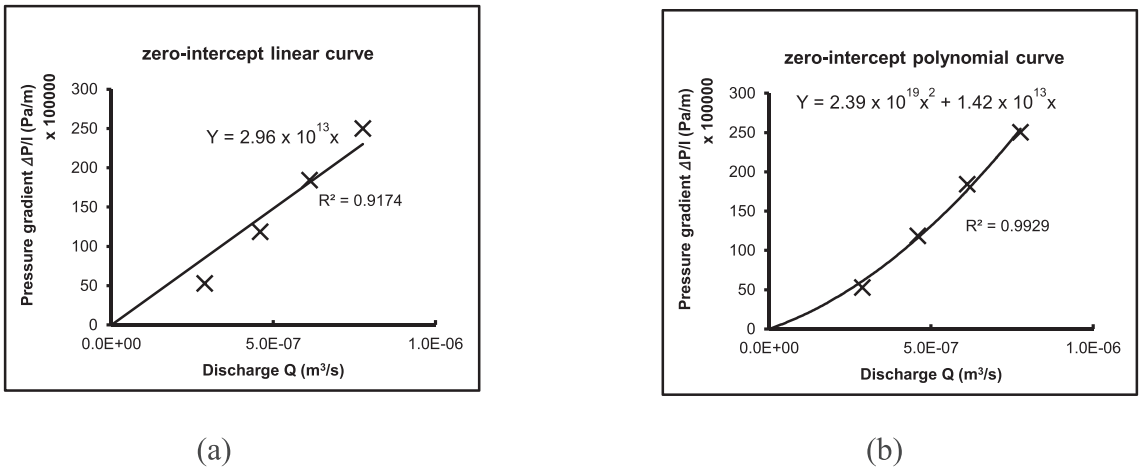

Fig. A2. Best fit Flow plots at 10 MPa confining pressure for the propped bituminous coal sample. a) zero-intercept linear curve, b) zero-intercept polynomial curve.

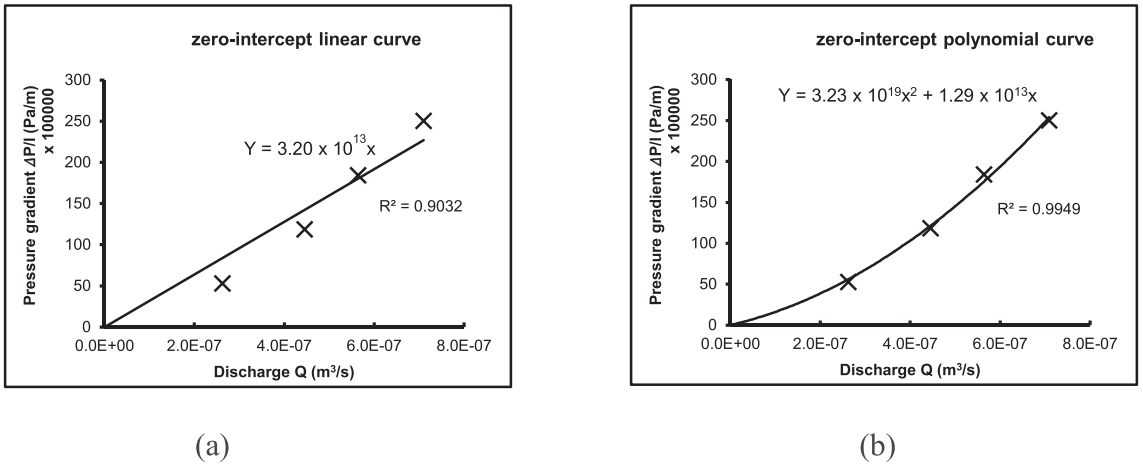

Fig. A3. Best fit Flow plots at 12 MPa confining pressure for the propped bituminous coal sample. a) zero-intercept linear curve, b) zero-intercept polynomial curve.

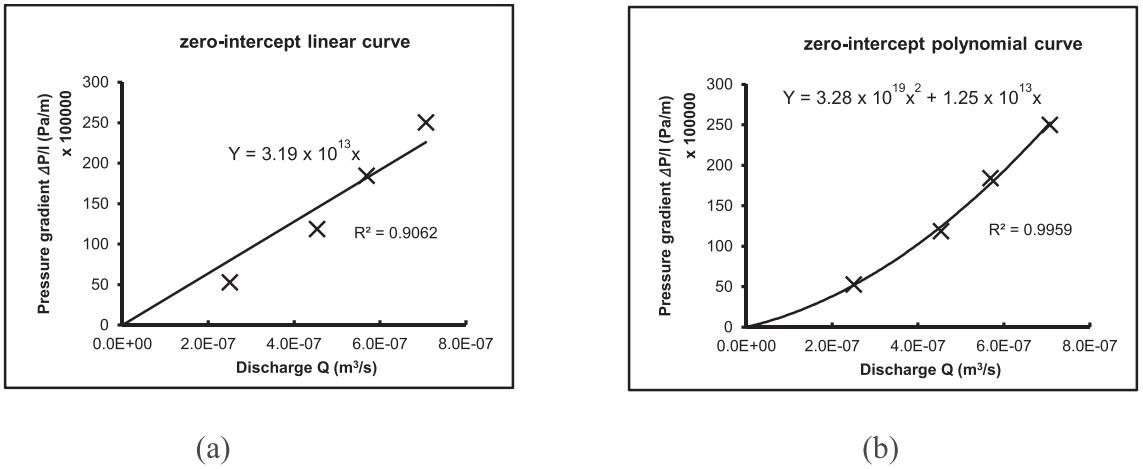

Fig. A4. Best fit Flow plots at 14 MPa confining pressure for the propped bituminous coal sample. a) zero-intercept linear curve, b) zero-intercept polynomial curve.

the primary parameters (the impact of proppants and coal maturity on fracture conductivity) of concern, which then can be comprehensively understood and interpret the relationship of these parameters on coal fracture flow. Nevertheless, for future work, new techniques can be implemented to investigate other parameters that may influence the propped and unpropped fracture flow behaviour in coal.

CRediT authorship contribution statement

M.A.A. Ahamed: Writing – original draft, Data curation. **M.S.A. Perera:** Conceptualization, Methodology. **D. Elsworth:** Writing – review & editing. **P.G. Ranjith:** Resources. **S.K.M. Matthai:** Validation. **Li Dong-yin:** Resources.

Declaration of Competing Interest

The authors declare that they have no known competing financial interests or personal relationships that could have appeared to influence the work reported in this paper.

Appendix A

Figs. A1–A4.

References

[1] Cheng J. Biomass to renewable energy processes. CRC Press; 2017.
[2] Ahamed MAA, Perera MSA, Matthai SK, Ranjith PG, Dong-yin Li. Coal composition and structural variation with rank and its influence on the coal-moisture interactions under coal seam temperature conditions–A review article. J Petrol Sci Eng 2019;180:901–17.
[3] Tasri A, Susilawati A. Selection among renewable energy alternatives based on a fuzzy analytic hierarchy process in Indonesia. Sustain Energy Technol Assess 2014; 7:34–44.
[4] Wanniarachchi W, Ranjith P, Perera M. Shale gas fracturing using foam-based fracturing fluid: a review. Environ Earth Sci 2017;76(2):91.
[5] Ranathunga AS, Perera MSA, Ranjith PG. Deep coal seams as a greener energy source: a review. J Geophys Eng 2014;11(6):063001. https://doi.org/10.1088/1742-2132/11/6/063001.
[6] Wu Y, Pan Z, Zhang D, Down DI, Lu Z, Connell LD. Experimental study of permeability behaviour for proppant supported coal fracture. J Nat Gas Sci Eng 2018;51:18–26.
[7] Weaver JD, Nguyen PD, Parker MA, van Batenburg DW. Sustaining fracture conductivity. SPE European Formation Damage Conference. Society of Petroleum Engineers; 2005.
[8] Xu T, Ranjith PG, Au ASK, Wasantha PLP, Yang TH, Tang CA, et al. Numerical and experimental investigation of hydraulic fracturing in Kaolin clay. J Petrol Sci Eng 2015;134:223–36.
[9] Liu H, Yang T, Xu T, Yu Q. A comparative study of hydraulic fracturing with various boreholes in coal seam. Geosci J 2015;19(3):489–502.
[10] Mahoney JV, Stubbs P, Schwerer III F, Dobscha F. Effects of a No-Proppant Foam Stimulation Treatment on a Coal-Seam Degasification Borehole. J Petroleum Technol 1981;33(11). 2,227-2,35.
[11] Hossain M, Rahman M, Rahman S. A shear dilation stimulation model for production enhancement from naturally fractured reservoirs. SPE J 2002;7(2): 183–95.
[12] Britt LK, Smith MB, Haddad ZA, Lawrence JP, Chipperfield ST, Waterfracs HTJ. We do need proppant after all. SPE Annual Technical Conference and Exhibition. Society of Petroleum Engineers; 2006.
[13] Ahamed MAA, Perera MSA, Dong-yin Li, Ranjith PG, Matthai SK. Proppant damage mechanisms in coal seam reservoirs during the hydraulic fracturing process: A review. Fuel 2019;253:615–29.
[14] Kravits S. Evaluation of Hydraulically-fractured In-Mine Horizontal Wells as a Completion Approach for Coalbed Methane Recovery Independent of and in Conjunction with Coal Mine Operations. REI Underground Exploration Draft Report. 1993.
[15] Jeffrey R, Boucher C. Sand Propped hydraulic fracture stimulation of horizontal in-seam gas drainage holes at Dartbrook Coal Mine; 2004.
[16] Kumar H, Elsworth D, Liu J, Pone D, Mathews JP. Permeability evolution of propped artificial fractures in coal on injection of CO2. J Petrol Sci Eng 2015;133: 695–704.
[17] Zimmerman RW, Bodvarsson GS. Hydraulic conductivity of rock fractures. Transp Porous Media 1996;23(1):1–30.
[18] Daneshy A. Horizontal well fracturing: A state-of-the-art report. World Oil 2013; 234(7):1–7.
[19] Wen Q, Zhang S, Wang L, Liu Y, Li X. The effect of proppant embedment upon the long-term conductivity of fractures. J Petrol Sci Eng 2007;55(3-4):221–7.
[20] Keshavarz A, Badalyan A, Johnson R, Bedrikovetsky P. Stimulation of Unconventional Reservoirs using Graded Proppant Injection. SPE Russian Petroleum Technology Conference. Society of Petroleum Engineers; 2015.
[21] Zimmerman RW, Kumar S, Bodvarsson GS. Lubrication theory analysis of the permeability of rough-walled fractures. Elsevier Int J Rock Mech Min Sci Geomech Abstr 1991;28(4):325–31.
[22] Liu E. Effects of fracture aperture and roughness on hydraulic and mechanical properties of rocks: implication of seismic characterization of fractured reservoirs. J Geophys Eng 2005;2(1):38–47.
[23] Cherubini C, Giasi C, Pastore N. Bench scale laboratory tests to analyze non-linear flow in fractured media. Hydrolo Earth Syst Sci 2012;16(8):2511–22.
[24] Nowamooz A, Radilla G, Fourar M. Non-Darcian two-phase flow in a transparent replica of a rough-walled rock fracture. Water Resour Res 2009;45(7).
[25] Fourar M, Bories S, Lenormand R, Persoff P. Two-phase flow in smooth and rough fractures: Measurement and correlation by porous-medium and pipe flow models. Water Resour Res 1993;29(11):3699–708.
[26] Ranjith PG, Viete DR. Applicability of the 'cubic law' for non-Darcian fracture flow. J Petrol Sci Eng 2011;78(2):321–7.
[27] Barton CM, Gloe CS, Holdgate GR. Latrobe Valley, Victoria, Australia: a world class brown coal deposit. Int J Coal Geol 1993;23(1-4):193–213.
[28] Daneshy A, Crichlow H. Numerical solution of sand transport in hydraulic fracturing. Duncan, OK: Halliburton Services; 1980.
[29] Gadde PB, Liu Y, Norman J, Bonnecaze R, Sharma MM. Modeling proppant settling in water-fracs. SPE annual technical conference and exhibition: Society of Petroleum Engineers; 2004.
[30] Stringfellow WT, Domen JK, Camarillo MK, Sandelin WL, Borglin S. Physical, chemical, and biological characteristics of compounds used in hydraulic fracturing. J Hazard Mater 2014;275:37–54.
[31] Zheng W, Tannant D. Frac sand crushing characteristics and morphology changes under high compressive stress and implications for sand pack permeability. Can Geotech J 2016;53(9):1412–23.
[32] Pan J, Zhang Z, Li M, Wu Y, Wang K. Characteristics of multi-scale pore structure of coal and its influence on permeability. Nat Gas Ind B 2019;6(4):357–65.
[33] Keshavarz A, Badalyan A, Carageorgos T, Bedrikovetsky P, Johnson R. Stimulation of coal seam permeability by micro-sized graded proppant placement using selective fluid properties. Fuel 2015;144:228–36.
[34] Khanna A, Keshavarz A, Mobbs K, Davis M, Bedrikovetsky P. Stimulation of the natural fracture system by graded proppant injection. J Petrol Sci Eng 2013;111: 71–7.
[35] Sanematsu P, Shen Y, Thompson K, Yu T, Wang Y, Chang D-L, et al. Image-based Stokes flow modeling in bulk proppant packs and propped fractures under high loading stresses. J Petrol Sci Eng 2015;135:391–402.
[36] Wang H, Sharma MM. Estimating un-propped fracture conductivity and fracture compliance from diagnostic fracture injection tests. arXiv preprint arXiv: 180205112 2018.
[37] Hopkins DL, Cook NG, Myer LR. Fracture stiffness and aperture as a function of applied stress and contact geometry. The 28th US Symposium on Rock Mechanics (USRMS). American Rock Mechanics Association; 1987.
[38] Pyrak-Nolte LJ, Nolte DD. Approaching a universal scaling relationship between fracture stiffness and fluid flow. Nat Commun 2016;7(1):1–6.
[39] Cheung B, Hilling S, Brierley SP. Impact of Low Cost Proppant and Fluid Systems in Hydraulic Fracturing of Unconventional Wells. Abu Dhabi International Petroleum Exhibition & Conference. Society of Petroleum Engineers; 2018.
[40] Ahamed MAA, Perera MSA, Black JR, Matthai SK, Ranjith PG, Dong-yin Li, et al. Investigating the proppant damage mechanisms expected in a propped coal fracture and its effect on fracture flow. J Petrol Sci Eng 2021;198:108170. https://doi.org/10.1016/j.petrol.2020.108170.
[41] Li K, Gao Y, Lyu Y, Wang M. New mathematical models for calculating proppant embedment and fracture conductivity. SPE J 2015;20(03):496–507.
[42] Chen M, Zhang S, Liu M, Ma X, Zou Y, Zhou T, et al. Calculation method of proppant embedment depth in hydraulic fracturing. Pet Explor Dev 2018;45(1): 159–66.
[43] Lacy LL, Rickards AR, Ali SA. Embedment and fracture conductivity in soft formations associated with HEC, borate and water-based fracture designs. SPE Annual Technical Conference and Exhibition. Society of Petroleum Engineers; 1997.
[44] Akrad OM, Miskimins JL, Prasad M. The effects of fracturing fluids on shale rock mechanical properties and proppant embedment. SPE Annual Technical Conference and Exhibition. Society of Petroleum Engineers; 2011.